Optical and Quantum Electronics (2020) 52:30
https://doi.org/10.1007/s11082-019-2142-z

All-optical NOR and XNOR logic gates at 2 Tb/s based on two-photon absorption in quantum-dot semiconductor optical amplifiers

Amer Kotb[1,2] · Chunlei Guo[1,3]

Received: 9 June 2019 / Accepted: 3 December 2019 / Published online: 13 December 2019

Abstract

Two-photon absorption (TPA) is a nonlinear absorption process in semiconductors, creating a fast phase change in a low-intensity probe beam. Placing quantum-dots (QDs), on the other hand, in the active region of semiconductor optical amplifiers (SOAs) results in SOAs shorter carrier recovery time and lower gain saturation. Thus, in this article, the physical advantages of both TPA and QDs have been combined to numerically investigate the performance of all-optical NOT-OR (NOR) and exclusive-NOR (XNOR) logic gates, incorporating in Mach–Zehnder interferometers at a data rate of 2 Tb/s. The output quality factor (QF) of the considered Boolean functions against the key operational parameters is assessed and examined, including the impact of amplified spontaneous emission in order to obtain more realistic results. The overall QF in the presence of TPA is always higher than that without TPA.

Keywords All-optical NOR logic gate · All-optical XNOR logic gate · Two-photon absorption · Quantum-dot semiconductor optical amplifier · Mach–Zehnder interferometer · Quality factor

1 Introduction

All-optical (AO) logic gates are essential elements for optical signal processing and high-speed optical networks. Semiconductor optical amplifiers (SOAs) have been widely used in recent years to demonstrate AO NOT-OR (NOR) and exclusive-NOR (XNOR) operations at different data rates (Byun et al. 2003; Sharaiha et al. 2006;Kim et al. 2004, 2006a, b;

✉ Amer Kotb
amer@ciomp.ac.cn

✉ Chunlei Guo
guo@optics.rochester.edu

1 The Guo China-US Photonics Laboratory, Changchun Institute of Optics, Fine Mechanics, and Physics, Chinese Academy of Sciences, Changchun 130033, China

2 Department of Physics, Faculty of Science, University of Fayoum, Fayoum 63514, Egypt

3 The Institute of Optics, University of Rochester, Rochester, NY 14627, USA

Xu et al. 2006; Sun et al. 2007; Dong et al. 2008; Chen et al. 2016; Kotb 2017a, b; Kotb et al. 2018; Han and Liu 2019; Lee et al. 2002; Kang et al. 1906; Singh and Lovkesh 2012; Zhang et al. 2019) owing to their strong nonlinearity, compactness, stability, and simplicity. It is well known that the SOAs have slow gain and phase recovery dynamics, which limit their applications in AO logic gates that hardly exceed ~ 100 Gb/s. On the other hand, the nonlinear effect of the two-photon absorption (TPA) can be used to overcome the SOAs physical limitations. The TPA provides extra-carriers in the SOA active regions that induce the ultrafast phase and gain changes of a weak probe signal for AO applications. Pump-probe experiments have confirmed that the phase changes take place in a duration of 1 ps or less when both pump and probe signals are launched into SOA (Dorren et al. 2003, 2004; Hong et al. 1996). The cross-phase modulation (XPM) between a high pump signal and a weak probe signal due to the TPA response can be utilized to realize AO NOR and XNOR operations at 250 Gb/s using SOAs as in (Kotb 2014, 2015). On the other hand, placing quantum-dots (QDs) in the SOA active region results in shorter carrier relaxation time and lower gain saturation (Dutta and Wang 2013). Furthermore, the QDSOAs have several improved characteristics compared with bulk or quantum-well SOAs such as high saturation power (Xiao and Huang 2008; Qasaimeh 2003), high-temperature stability (Sugawara et al. 2005; Grillot et al. 2009), wide gain bandwidth (Akiyama et al. 2005; Meuer et al. 2010), low noise figure (Xiao and Huang 2008; Bilenca and Eisenstein 2004), and, above of all, the ultrafast gain response (Berg et al. 2011; van der Poel et al. 2005; Kim et al. 2009; Zilkie et al. 2007). All of these features make the QDSOAs a promising component in applications of AO NOR and XNOR gates at different data rates up to 1 Tb/s (Dimitriadou and Zoiros 2012a, b, 2013; Kotb 2013, 2015; Kotb and Zoiros 2013; Li et al. 2015; Hu et al. 2017). In this article, the advantages of both TPA and QD in SOAs have been combined to extend and continue the previous relevant works (Zhang and Dutta 2018; Thapa et al. 2019; Kotb et al. 2019; Kotb and Guo 2019) through a numerical investigation of AO NOR and XNOR operations at 2 Tb/s. The unit switching device used for implementing these Boolean functions is Mach–Zehnder interferometer (MZI), which has two symmetrical QDSOAs in each arm where it's easy to control the signal phase. The MZI is a promising element due to its attractive features such as a simple structure, high stability, efficient operation, and easy implementation (Han and Liu 2019; Dutta and Wang 2013). This device has been named in 1892 for the two physicists Ludwig Mach and Ludwig Zehnder (Pereira et al. 2009). The effect of the input pulse and QDSOA key parameters on the gate's output quality factor (QF) with and without TPA is examined and assessed, including the impact of amplified spontaneous emission (ASE) in order to obtain more realistic results. The achieved results confirm that using QDSOA with TPA at 2 Tb/s achieves both logical correctness and higher QF than without TPA.

The rest of this paper is organized as follows: In Sect. 2, the QDSOA rate equations are formulated. In Sect. 3, the NOR operation principle, results, and discussions are described. In Sect. 4, the XNOR operation principle, results, and discussions are presented. Finally, the concluding remarks are given in Sect. 5.

2 QDSOA rate equations

The QDSOAs device used in this simulation to construct the AO NOR and XNOR gates is the commonly discussed InAs/GaAs where InAs QDs embedded in GaAs layers (Zhang and Dutta 2018; Thapa et al. 2019; Kotb et al. 2019; Kotb and Guo 2019). This device has gain ~ 15 dB and noise figure ~ 7 dB around 1.55 μm wavelength (Zhang and Dutta 2018; Thapa et al. 2019). Figure 1 shows schematically the QD carrier dynamics under TPA in QDSOA (Zhang and Dutta 2018; Thapa et al. 2019; Kotb et al. 2019; Kotb and Guo 2019). The amplification process depletes the carriers in QDs, while the carriers generated by the injection current and TPA also provides extra-carriers on picosecond timescales by carrier-relaxation from bulk region to QDs via the wetting layer (WL). The carriers injected into the WL by the injection current make a transition to the QD excited state (ES) followed by a transition to the QD ground state (GS). The extra-carriers generated by the TPA effect enhance the QDs carrier capture rate and result in much-reduced pattern effects dependence of the QDs carrier recovery dynamics compared with the case without the TPA effect (Ju et al. 2006).

The following coupled first-order differential equations describe the change in the QDSOA carrier dynamics among a two-level model, taking into account the nonlinear intraband effects of spectral hole burning (SHB) and carrier heating (CH), which occur on ultrafast timescales (Kotb 2013; Kotb and Zoiros 2013; Kotb et al. 2019; Kotb and Guo 2019):

$$\frac{dh_d(t)}{dt} = \frac{h_w(t)}{\tau_{dw}}\left(1 - \frac{h_d(t)}{h_0}\right) - \frac{h_d(t)}{\tau_{dr}} - \left(\exp\left[h_d(t) + h_{CH}(t) + h_{SHB}(t)\right] - 1\right)\frac{P_{in}(t)}{E_{sat}} \tag{1}$$

$$\frac{dh_w(t)}{dt} = \frac{h_{in}}{\tau_{wr}}\left(1 - \frac{h_w(t)}{h_0}\right) - \frac{h_w(t)}{\tau_{wr}} - \frac{h_w(t)}{\tau_{wd}}\left(1 - \frac{h_d(t)}{h_0}\right) \tag{2}$$

$$\frac{dh_{CH}(t)}{dt} = -\frac{h_{CH}(t)}{\tau_{CH}} - \frac{\varepsilon_{CH}}{\tau_{CH}}\left(\exp\left[h_d(t) + h_{CH}(t) + h_{SHB}(t)\right] - 1\right)P_{in}(t) \tag{3}$$

$$\frac{dh_{SHB}(t)}{dt} = -\frac{h_{SHB}(t)}{\tau_{SHB}} - \frac{\varepsilon_{SHB}}{\tau_{SHB}}\left(exp\left[h_d(t) + h_{SHB}(t) + h_{CH}(t)\right] - 1\right)P_{in}(t) - \frac{dh_d(t)}{dt} - \frac{dh_{CH}(t)}{dt} \tag{4}$$

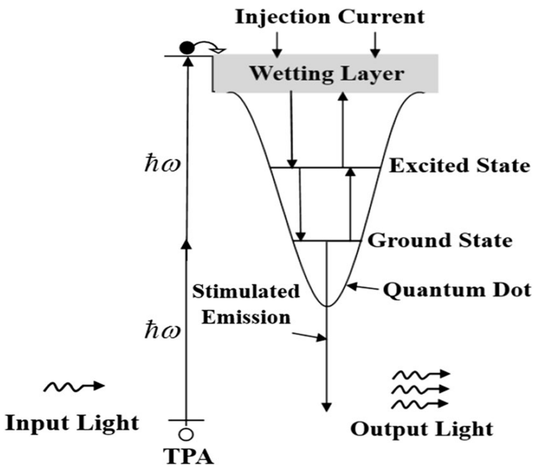

Fig. 1 Schematic of QDs carrier dynamics under TPA in QDSOA

$$h_{in} = \int_0^z \frac{aJ\tau_{wr}}{ed}\, dz' \tag{5}$$

where h(t) represents the integral of QDSOA optical gain over the longitudinal dimension, z, for the carrier recombination between QDs states (h_d), WL (h_w), carrier heating (h_{CH}), and spectral hole burning (h_{SHB}). $h_0 = \ln[G_0]$, where G_0 is the unsaturated power gain, $P_{in}(t)$ is the input signal power, and E_{sat} is the saturation energy. τ_{dw} is the excitation rate from QD GS to WL and τ_{wd} is the transition rate from WL to QD GS. τ_{dr} is the QD carrier recombination rate and τ_{wr} is the WL carrier recombination rate. τ_{CH} is the temperature relaxation rate and τ_{SHB} is the carrier–carrier scattering rate. ε_{CH} and ε_{SHB} are the nonlinear gain suppression factors due to CH and SHB, respectively. ɑ is the differential gain, which is the ratio of the carrier in WL and QDs, J is the injection current density, d is the thickness of WL, and e is the electron charge. The total optical gain of each QDSOA equals the sum of h_d, h_{CH}, and h_{SHB}, i.e.

$$G_{QDSOA}(t) = \exp\left[h_d(t) + h_{CH}(t) + h_{SHB}(t)\right] \tag{6}$$

The total phase change of the probe wave propagated in each QDSOA, including the TPA effect is given by (Kotb et al. 2019; Kotb and Guo 2019; Zhang et al. 2015):

$$\Phi_{QDSOA}(t) = -0.5\left(\alpha\, h_d\,(t) + \alpha_{CH} h_{CH}(t) + \beta\, \alpha_{TPA}\, L\, S(t)\right) \tag{7}$$

where α is the traditional linewidth enhancement factor (α-factor) and α_{CH} is the linewidth enhancement factor due to CH. The value of the linewidth enhancement factor due to SHB (α_{SHB}) is zero because the SHB produces a nearly symmetrical spectral hole centered at the signal wavelength (Kotb 2013). β is the TPA coefficient and α_{TPA} is the linewidth enhancement factor due to TPA. β has a typical value within the range of 20–35 cm/GW and experimentally derived α_{TPA} value is within the range of 4–5 for most semiconductors (Folliot et al. 2002; Dorren et al. 2002). L is the length of the QDSOA active region and S(t) is the light intensity (i.e. power density).

The modulation format of the input data pulse used in this simulation is a return-to-zero, which is widely used in the optical time-division multiplexing systems because of its efficient tolerance to fiber nonlinearity and higher receiver sensitivity (Breuer and Petermann 1997). This pulse is assumed to be a Gaussian-shaped whose power profile described by (Dutta and Wang 2013):

$$P_{A,B,Clk}(t) \equiv P_{in}(t) = \sum_{n=1}^{N} a_{n(A,B,Clk)} \frac{2\sqrt{\ln[2]}\, E_0}{\sqrt{\pi}\, \tau_{FWHM}} \exp\left[-\frac{4\ln[2](t-nT)^2}{\tau_{FWHM}^2}\right] \tag{8}$$

where $an_{(A,B,Clk)}$ is the nth data of signals A and B where $an_{(A,B)}$ is '1' or '0' and a clock (Clk) signal where $a_{n(Clk)}$ is '1' inside $N = 2^7 - 1$ (Kotb and Guo 2019; Zhang et al. 2015) bits-long pseudorandom binary sequence (PRBS) of pulses having an energy E_0, bit period T, and full-width at half-maximum (FWHM) pulse width τ_{FWHM}. The QDSOAs differential rate Eqs. (1)–(4) have been numerically solved using Adams' method in Mathematica Wolfram® for the default parameters cited in Table 1. There are two conditions which are definitely applied: First, the incident power at the beginning of time, i.e. at t = 0, is Gaussian, and second, $h_0(t = 0) = \ln[G_{SS}]$, where G_{SS} is the small-signal gain. These are applied to Eq. (1)–(5), with the appropriate adjustment for the rest of the 'h' functions, i.e. they have not been perturbed yet until a pulse arrives. The quality of the considered Boolean

Table 1 Calculation default parameters

Symbol	Definition	Value	Unit	Reference
E_0	Pulse energy	0.3	pJ	–
τ_{FWHM}	Pulse width	0.2	ps	(Kotb et al. 2019; Kotb and Guo 2019)
T	Bit period	0.5	ps	(Kotb et al. 2019; Kotb and Guo 2019)
N	PRBS length	127	–	(Kotb et al. 2019; Kotb and Guo 2019)
λ_A	Wavelength of signal A (NOR gate)	1545	nm	(Sun et al. 2007; Dutta and Wang 2013)
λ_B	Wavelength of signal B (NOR gate)	1545	nm	(Sun et al. 2007; Dutta and Wang 2013)
λ_{Clk}	Wavelength of Clk signal (NOR gate)	1555	nm	(Sun et al. 2007; Dutta and Wang 2013)
λ_{CW}	Wavelength of CW (NOR gate)	1550	nm	(Sun et al. 2007; Dutta and Wang 2013)
P_A	Power of signal A (NOR gate)	2	mW	(Sun et al. 2007)
P_B	Power of signal B (NOR gate)	2	mW	(Sun et al. 2007)
P_{Clk}	Power of Clk signal (NOR gate)	2	mW	(Sun et al. 2007)
P_{CW}	Power of CW (NOR gate)	1	mW	(Sun et al. 2007)
λ_A	Wavelength of signal A (XNOR gate)	1545	nm	(Kotb 2012)
λ_B	Wavelength of signal B (XNOR gate)	1550	nm	(Kotb 2012)
λ_{Clk}	Wavelength of Clk signal (XNOR gate)	1553.8	nm	(Lee et al. 2002)
λ_{CW}	Wavelength of CW (XNOR gate)	1545	nm	(Lee et al. 2002)
P_A	Power of signal A (XNOR gate)	1	mW	(Wang et al. 2004)
P_B	Power of signal B (XNOR gate)	1	mW	(Wang et al. 2004)
P_{Clk}	Power of Clk signal (XNOR gate)	2	mW	(Lee et al. 2002)
P_{CW}	Power of CW (XNOR gate)	2	mW	(Wang et al. 2004)
β	Coefficient of TPA	30	cm/GW	(Kotb 2015; Kotb and Guo 2019; Sun et al. 2005)
α_{TPA}	Linewidth enhancement factor due to TPA	4	–	(Kotb 2015; Li et al. 2012)
J	Injection current density	10	kA/cm^2	–
P_{sat}	Saturation power	30	mW	(Kotb et al. 2019; Kotb and Guo 2019)
τ_{wd}	Transition rate from WL to QDs state	5	ps	(Dutta and Wang 2013; Dimitriadou and Zoiros 2012; Kotb 2013; Kotb and Zoiros 2013)
τ_{dw}	Excitation rate from QDs state to WL	10	ns	(Dutta and Wang 2013; Dimitriadou and Zoiros 2012; Kotb 2013; Kotb and Zoiros 2013)
τ_{wr}	Carrier recombination rate in WL	2.2	ns	(Dutta and Wang 2013; Dimitriadou and Zoiros 2012; Kotb 2013; Kotb and Zoiros 2013)

Table 1 (continued)

Symbol	Definition	Value	Unit	Reference
τ_{dr}	Carrier recombination rate in QDs state	0.4	ns	(Dutta and Wang 2013; Dimitriadou and Zoiros 2012; Kotb 2013; Kotb and Zoiros 2013)
τ_{CH}	Temperature relaxation rate	0.3	ps	(Dutta and Wang 2013; Dimitriadou and Zoiros 2012; Kotb 2013; Kotb and Zoiros 2013)
τ_{SHB}	Carrier-carrier scattering rate	0.1	ps	(Dutta and Wang 2013; Dimitriadou and Zoiros 2012; Kotb 2013; Kotb and Zoiros 2013)
α	Traditional α-factor	2	–	(Kotb 2015)
α_{CH}	Linewidth enhancement factor due to CH	1	–	(Kotb et al. 2019; Kotb and Guo 2019)
α_{SHB}	Linewidth enhancement factor due to SHB	0	–	(Wang et al. 2004)
ε_{CH}	Nonlinear gain suppression factor due to CH	0.2	W^{-1}	(Dutta and Wang 2013)
ε_{SHB}	Nonlinear gain suppression factor due to SHB	0.2	W^{-1}	(Dutta and Wang 2013)
Γ	Confinement factor	0.15	–	(Kotb et al. 2019; Kotb and Guo 2019)
a	Differential gain	8.6×10^{-15}	cm^2	(Li et al. 2015; Hu et al. 2017; Zhang and Dutta 2018; Thapa et al. 2019; Kotb et al. 2019; Kotb and Guo 2019; Ma et al. 2009)
L	Length of QDSOA active region	1.0	mm	(Li et al. 2015; Hu et al. 2017; Zhang and Dutta 2018; Thapa et al. 2019; Kotb et al. 2019; Kotb and Guo 2019)
W	Thickness of QDSOA active region	0.3	µm	(Kotb et al. 2019; Kotb and Guo 2019)
d	Thickness of WL	0.5	µm	(Kotb and Guo 2019)
G_0	Unsaturated power gain	30	dB	(Kotb and Guo 2019; Wang et al. 2004)
B_0	Optical bandwidth	3	nm	(Kotb and Guo 2019)
υ	Optical frequency	1550	nm	(Kotb and Guo 2019)
N_{SP}	Spontaneous emission factor	2	–	(Kotb et al. 2019; Kotb and Guo 2019)

functions has been examined by the output QF, which is defined as $QF = (P_1 - P_0)/(\sigma_1 + \sigma_0)$ (Dutta and Wang 2013), where $P_{1,0}$ and $\sigma_{1,0}$ are the average peak powers and corresponding standard deviations, respectively, of binary values '1' and '0'.

3 NOR gate

3.1 Operation principle

The output of the NOR gate gives only '1' output when both inputs are '0' and it's logically an inverted OR gate. The schematic diagram and corresponding truth table of the NOR gate using QDSOAs-MZI are illustrated in Fig. 2.

In order to realize NOR operation, data signals A and B and clock (Clk) signal are combined using a wavelength selective coupler (WSC) and launched into the upper and lower arms of QDSOAs-MZI, respectively, while a continuous-wave (CW) probe signal is injected into the middle arm of QDSOAs-MZI via a 3 dB optical coupler. Signals A and B combinations ('00', '01', '10', and '11') and the Clk signal (all '1') will modulate the gains of the upper and lower arms, respectively, and thereby the phase of the CW probe signal injected into the middle arm. Furthermore, when the data signals A and B combinations ('01', '10', or '11') are launched into QDSOA1 and the Clk signal (all '1') is launched into QDSOA2, both QDSOAs become saturated, therefore the modulated CW probe phase will be equal ('1' state) after each arm, which results in a destructive interferences ('0') at the output port of QDSOAs-MZI. When the signals A and B combination ('00') is injected, there is no phase balance in the two arms due to the Clk signal; hence, a logic '1' is obtained at the QDSOAs-MZI output due to constructive interference. In this manner, the NOR operation is achieved between the binary contents of signals A and B according to the NOR truth table.

3.2 Simulation and results

The total input power going into QDSOA1 and QDSOA2 is given, respectively, by:

$$P_{in,\mathrm{QDSOA1}}(t) = P_A(t) + P_B(t) + 0.5P_{CW} \tag{9}$$

$$P_{in,\mathrm{QDSOA2}}(t) = P_{Clk}(t) + 0.5P_{CW} \tag{10}$$

where the coefficient '0.5' refers to the halving of signal CW coupled into the middle arm of QDSOAs-MZI via 3 dB OC.

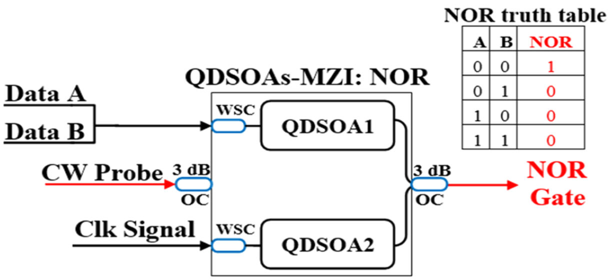

Fig. 2 Schematic diagram and truth table of NOR gate using QDSOAs-MZI. *OC* 3 dB optical coupler. *WSC* wavelength selective coupler

The NOR output power coming out of QDSOAs-MZI, including the ASE effect, is given by (Dimitriadou and Zoiros 2012; Kotb 2013):

$$P_{out,NOR}(t) = 0.25\, P_{CW} \left(\begin{array}{r} G_{QDSOA1}(t) + G_{QDSOA2}(t) - 2\sqrt{G_{QDSOA1}(t)\, G_{QDSOA2}(t)} \\ \cos[\Phi_{QDSOA1}(t) - \Phi_{QDSOA2}(t)] \end{array} \right) + P_{ASE} \tag{11}$$

where $G_{QDSOA1,2}(t)$ and $\Phi_{QDSOA1,2}(t)$ are, respectively, the time-dependent gains and phase changes of the QDSOAs-MZI arms. P_{ASE} is the ASE power, which is related to the spontaneous emission factor (N_{SP}) through $P_{ASE} = N_{SP}\,(G_0 - 1)\; 2\pi\hbar\upsilon B_0$ (Kotb 2015; Dutta and Wang 2013; Kotb and Guo 2019), where ħ is normalized Planck's constant, υ is the optical frequency, and B_0 is the optical bandwidth.

Figure 3 shows the calculated change in the gain of the NOR gate as a function of time at a pulse train of 2 Tb/s injected into QDSOAs without and with TPA effects.

Figures 4 and 5 illustrate the pulses' profile and corresponding eye diagrams of the NOR operation using QDSOAs-MZI at 2 Tb/s with and without TPA, respectively. The TPA induces a fast-phase modulation resulting in a small pattern effect with a higher QF than without TPA, i.e. 9.6 versus 4.8. The acceptable QF that keeps the related bit-error-rate (BER) less than 10^{-9} must be over 6 (Dutta and Wang 2013; Zhang and Dutta 2018; Thapa et al. 2019; Kotb et al. 2019; Kotb and Guo 2019) and that is the case in the presence of TPA. The BER is related to QF through $BER = (2\pi)^{-1/2} \exp[-0.5\, QF^2]/QF$ (Zhang and Dutta 2018; Thapa et al. 2019).

The calculated QF dependence on the input data A, B peak power and operating data rate for the NOR operation using QDSOAs-MZI at 2 Tb/s with and without TPA is shown, respectively, in Fig. 6a, b. In the presence of TPA, the QF is always higher than in the absence of TPA. The TPA effect is very sensitive to the input power value. Physically, at low input power, the phase change due to TPA effects is small and the pattern effects become more significant to degrade the QF. As the input power increases, the peak power is large enough to cause significant TPA and induces a fast phase modulation of the weak probe signal and the pattern effect becomes relatively small resulting in a higher QF. In the absence of TPA, on the other hand, a high input power depletes the carrier density via the stimulated emission that, in turn, causes a stronger pattern effect and accordingly a lower QF. The QF drops at high data rates, as shown in Fig. 6b, but its value remains acceptable

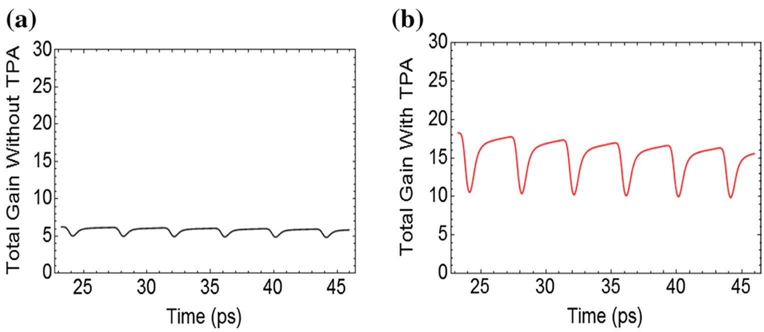

Fig. 3 Calculated change in gain of NOR gate as a function of time using QDSOAs at 2 Tb/s **a** without TPA and **b** with TPA

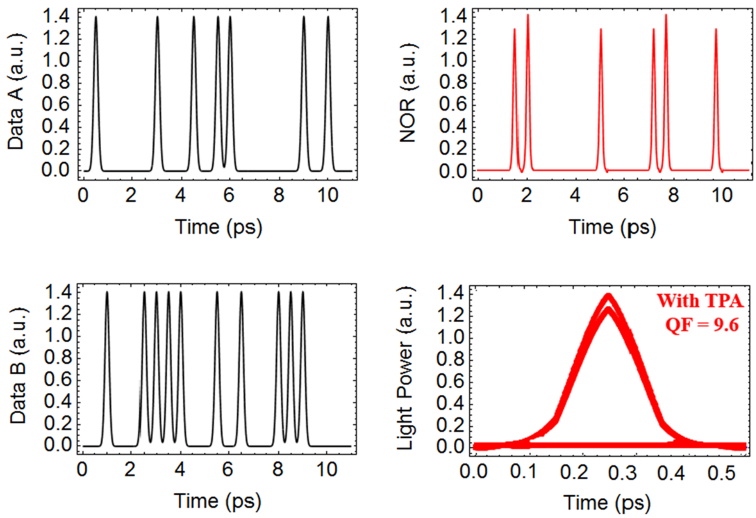

Fig. 4 Pulses' profile and corresponding eye diagram of NOR operation using QDSOAs-MZI at 2 Tb/s with TPA

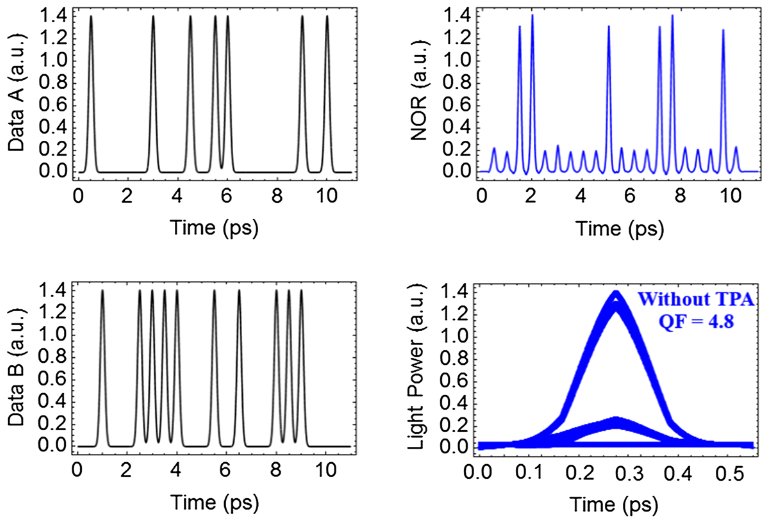

Fig. 5 Pulses' profile and corresponding eye diagram of NOR operation using QDSOAs-MZI at 2 Tb/s without TPA

(>6) in the presence of TPA even up to ~ 2.5 Tb/s, while this is impossible achieved without TPA. These results indicate that the TPA plays an important role in improving the QF and reducing the pattern effect in applications of ultrafast AO operations.

The NOR calculated QF versus the injection current density (J) and QDSOA confinement factor (Γ) using QDSOAs-MZI at 2 Tb/s with and without TPA is shown in Fig. 7a, b, respectively. From Fig. 7a, J is increased when more carriers produced in the WL, thus the carrier recovery time becomes faster, resulting in a higher QF for both with and without

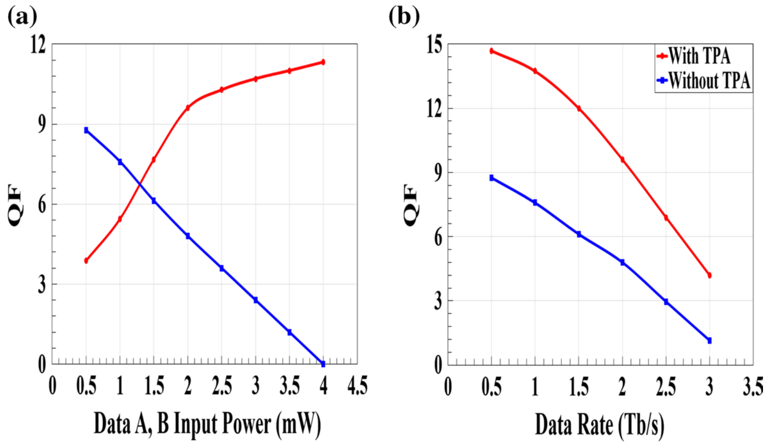

Fig. 6 Calculated QF of NOR gate as a function of **a** data A, B input peak power and **b** data rate using QDSOAs-MZI at 2 Tb/s with and without TPA

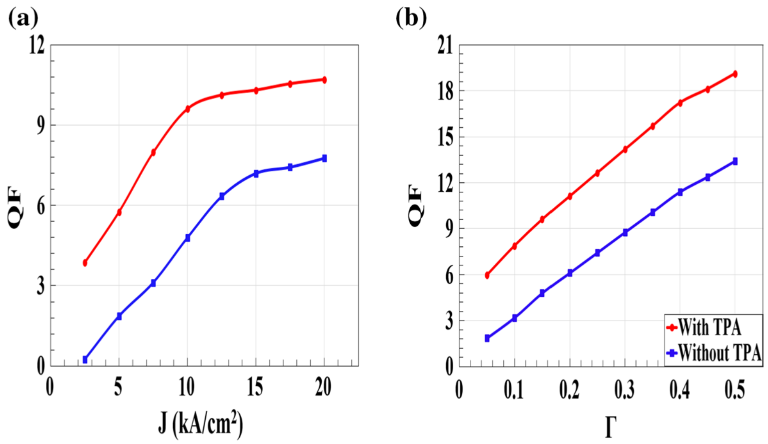

Fig. 7 Calculated QF of NOR gate versus **a** injection current density (J) and **b** confinement factor (Γ) using QDSOAs-MZI at 2 Tb/s with and without TPA

TPA cases. The TPA also accelerates much more the carrier recovery time, and thus the QF can saturate at a lower current level as shown in Fig. 7a than without TPA, i.e. 10 kA/cm^2 versus 15 kA/cm^2. A similar trend is seen in Fig. 7b where the QF is reduced for low values of Γ in both with and without cases. The QF with TPA is more acceptable, even for smaller values of Γ than without TPA.

The ASE causes additional noise through spontaneous–spontaneous beat noise and signal–spontaneous beat noise, which negatively affects the performance of the optical amplifiers, thus causing a QF degradation. The ASE causes a serious problem as a noise effect in SOAs since it's incoherent and limits the SOAs performance. Therefore, a mechanism should be employed to extract the ASE incoherent power, otherwise, the excited carriers in the active region will be depleted by the ASE effect. Thus, here, a 3 dB OC is used at the output of QDSOAs-MZI-based NOR/XNOR operation to separate the coherent signal

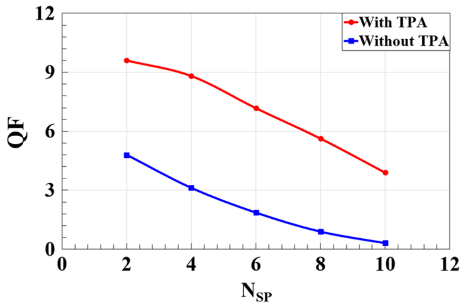

Fig. 8 Calculated QF of NOR gate as a function of spontaneous emission factor (N_{SP}) using QDSOAs-MZI at 2 Tb/s with and without TPA

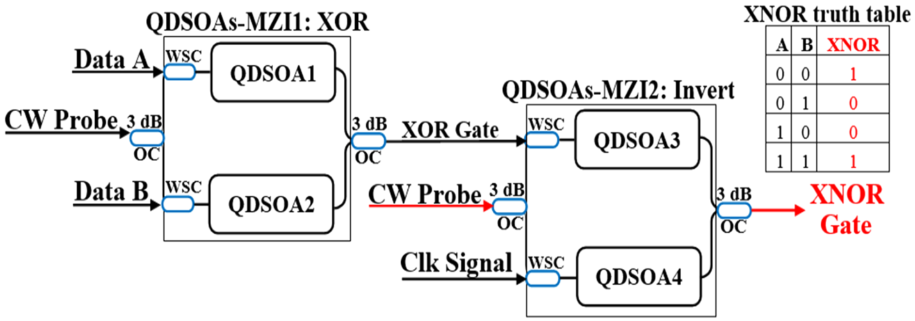

Fig. 9 Schematic diagram and corresponding truth table of XNOR gate using QDSOAs-MZIs. *OC* 3 dB optical coupler. *WSC* wavelength selective coupler

power from any ASE incoherent power, which does not have this too much affect internally the QDSOA fast gain dynamics in the presence of TPA. In this part, the impact of ASE noise on the QF is taken into account in order to obtain more realistic results. The ASE power is numerically added to the NOR output power as mentioned in Eq. (11). The QF drops with increasing N_{SP} in the presence and absence of TPA effects as shown in Fig. 8, while it is still having acceptable value in the presence of TPA using QDs active region even at a higher value of N_{SP}, i.e. ~ 6.

4 XNOR gate

4.1 Operation principle

The output of the XNOR gate is ‘1’ when all of its inputs are ‘1’ or when all of its inputs are ‘0’ and it’s logically an inverted XOR gate. The XNOR schematic diagram and corresponding truth table using QDSOAs-MZIs are illustrated in Fig. 9.

As shown in Fig. 9, the XNOR gate is realized by a series combination of the XOR gate using QDSOAs-MZI1 and Invert gate using QDSOAs-MZI2 (Kotb and Zoiros 2013; Kotb 2015). For XOR operation, the two input binary data streams A and B are combined and coupled via WSCs into the QDSOA1 and QDSOA2, respectively, while a CW probe signal is coupled via 3 dB OC into the middle port of the QDSOAs-MZI1. The data signals A and B induce a phase change in the CW probe signal via XPM in order to take the advantages of better performance and higher power efficiency than a cross-gain modulation (Durhuus et al. 1996). When both signals A and B are ‘0’, the CW probe signal traveling through the two arms of QDSOAs-MZI1 does not acquire any phase change resulting in ‘0’ at the QDSOAs-MZI1 output. When both signals A and B signals are ‘1’, the phase changes induced on the CW signal traveling through the two arms of QDSOAs-MZI1 are equal, resulting also in ‘0’ at the output port of the QDSOAs-MZI1. However, when A is ‘1’ and B is ‘0’, the CW suffers a phase change due to XPM in the upper arm of QDSOAs-MZI1 with signal A, resulting in ‘1’ at the QDSOAs-MZI1 output. The same output, i.e. ‘1’, is achieved when A is ‘0’ and B is ‘1’. In this manner, the XOR gate is achieved between the binary contents of signals A and B. For the Invert operation, the XOR coming out of QDSOAs-MZI1 and Clk signal are combined and coupled via WSCs into QDSOA3 and QDSOA4, respectively, while a CW probe signal is coupled via a 3 dB OC. The Clk signal is used to invert the XOR gate, so the output of QDSOAs-MZI2 is the XNOR operation according to its corresponding truth table.

4.2 Simulation and results

The total input power coupled into QDSOA1 and QDSOA2 of QDSOAs-MZI1 in order to realize the XOR operation is given, respectively, by:

$$P_{in,\,\mathrm{QDSOA1}}(t) = P_A(t) + 0.5P_{CW} \tag{12}$$

$$P_{in,\,\mathrm{QDSOA2}}(t) = P_B(t) + 0.5P_{CW} \tag{13}$$

The output power of the XOR operation coming out of QDSOAs-MZI1, including the ASE effect, is given by (Kotb et al. 2018):

$$P_{out,XOR}(t) = 0.25\,P_{CW}\left(\begin{array}{r} G_{QDSOA1}(t) + G_{QDSOA2}(t) - 2\sqrt{G_{QDSOA1}(t)\,G_{QDSOA2}(t)} \\ cos[\Phi_{QDSOA1}(t) - \Phi_{QDSOA2}(t)] \end{array}\right) + P_{ASE} \tag{14}$$

The total input power coupled into QDSOA3 and QDSOA4 of QDSOAs-MZI2 for XNOR operation is given, respectively, by:

$$P_{in,\,\mathrm{QDSOA3}}(t) = P_{out,XOR}(t) + 0.5P_{CW} \tag{15}$$

$$P_{in,\,\mathrm{QDSOA4}}(t) = P_{Clk}(t) + 0.5P_{CW} \tag{16}$$

The output power of the XNOR operation coming out of QDSOAs-MZIs, including the ASE effect, is given by (Kotb 2014, 2015; Kotb and Zoiros 2013):

$$P_{out,XNOR}(t) = 0.25\,P_{CW}\left(\begin{array}{r} G_{QDSOA3}(t) + G_{QDSOA4}(t) - 2\sqrt{G_{QDSOA3}(t)\,G_{QDSOA4}(t)} \\ cos\,[\Phi_{QDSOA3}(t) - \Phi_{QDSOA4}(t)] \end{array}\right) + P_{ASE} \tag{17}$$

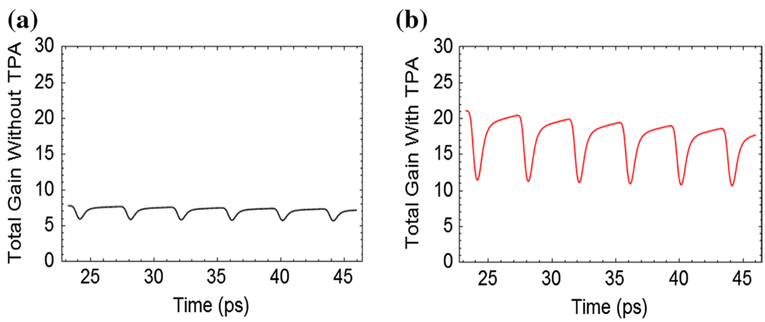

Fig. 10 Calculated change in gain of XNOR gate as a function of time using QDSOAs at 2 Tb/s **a** without TPA and **b** with TPA

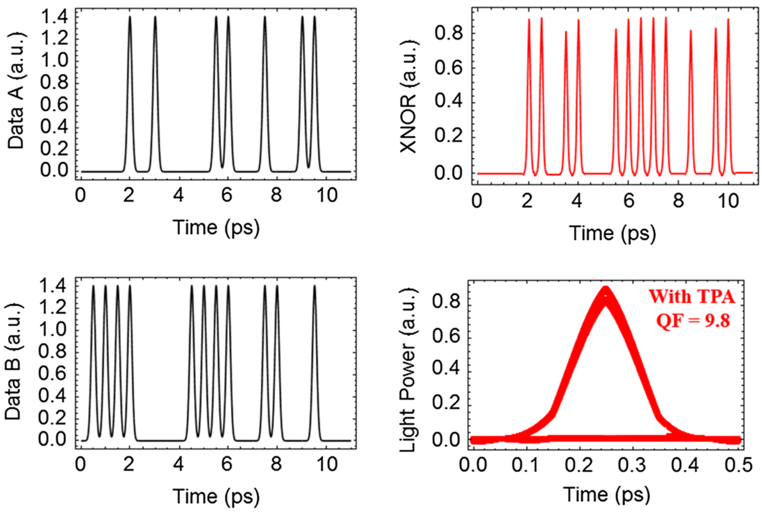

Fig. 11 Pulses' profile and corresponding eye diagram of XNOR operation using QDSOAs-MZIs at 2 Tb/s with TPA

The calculated changes in the gain of the XNOR gate as a function of time when a pulse train of 2 Tb/s is injected into QDSOAs without and with TPA effects is shown in Fig. 10a and b, respectively.

The pulses' profile and corresponding eye diagram of the XNOR operation using QDSOAs-MZIs at 2 Tb/s with and without TPA are illustrated, respectively, in Figs. 11 and 12. The achieved QF is 9.8 with TPA and 4.5 without TPA. Furthermore, the eye diagram without TPA is distorted due to high pattern effects, nevertheless, with TPA, it is clear and open.

The XNOR calculated QF against the input data A, B peak power and operating data rate using QDSOAs-MZIs at 2 Tb/s with and without TPA is shown in Fig. 13a, b, respectively. These results have been numerically obtained in the same way as described for the NOR operation.

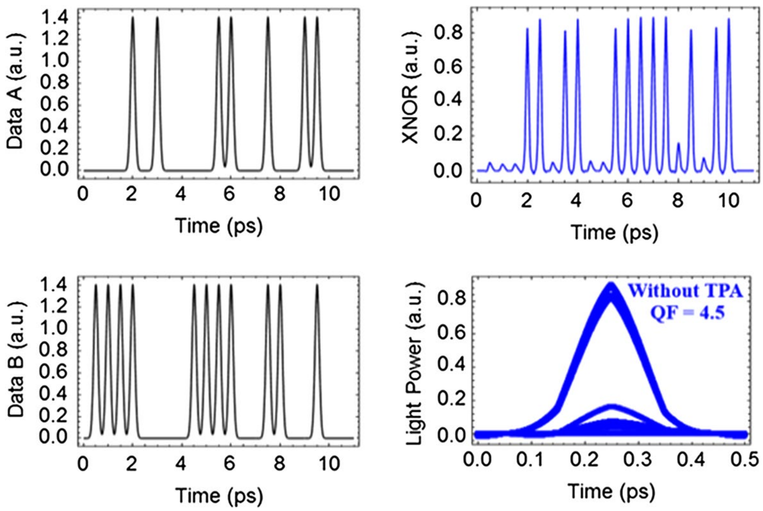

Fig. 12 Pulses' profile and corresponding eye diagram of XNOR operation using QDSOAs-MZIs at 2 Tb/s without TPA

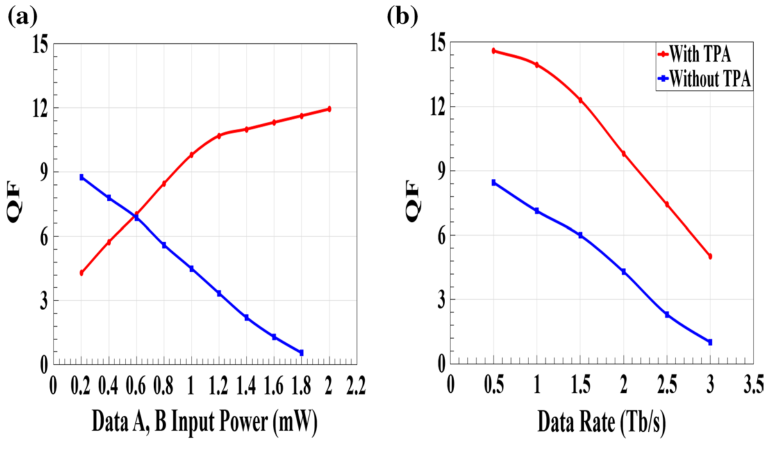

Fig. 13 Calculated QF of XNOR gate as a function of **a** data A, B input peak power and **b** data rate using QDSOAs-MZIs at 2 Tb/s with and without TPA

The dependence of the XNOR QF on the injection current density (J) and QDSOA confinement factor (Γ) using QDSOAs-MZIs at 2 Tb/s with and without TPA is shown, respectively, in Fig. 14a, b.

Figure 15 shows the QF as a function of N_{SP} of the XNOR operation at 2 Tb/s using QDSOAs-MZI with and without TPA.

The recent applications of high-speed AO NOR and XNOR gates are very useful in digital systems. In particular, the NOR gates are so-called 'universal gates, spanning from synthesizing any Boolean function (Xu et al. 2008) to building combinational

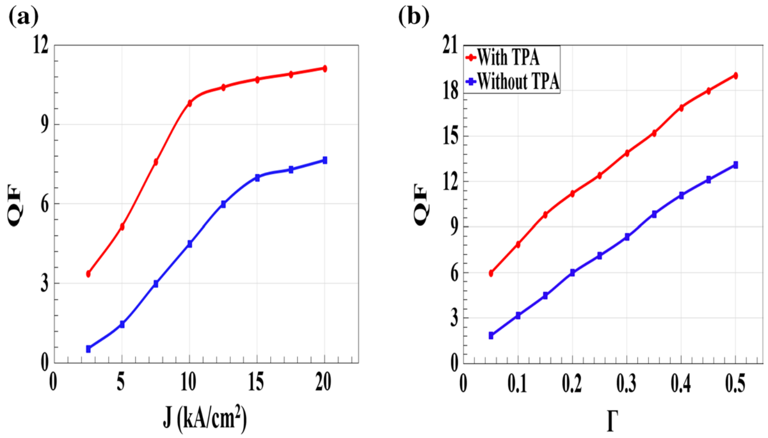

Fig. 14 Calculated QF of XNOR gate versus **a** injection current density (J) and **b** confinement factor (Γ) using QDSOAs-MZIs at 2 Tb/s with and without TPA

Fig. 15 Calculated QF of XNOR gate as a function of spontaneous emission factor (N_{SP}) at 2 Tb/s using QDSOAs-MZIs with and without TPA

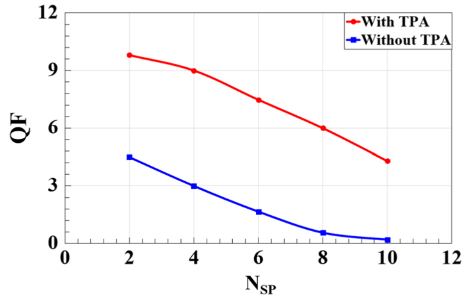

photonic logic circuits (Jung et al. 2008) and managing packet contention (Scaffardi et al. 2007) to bit-error monitoring (Chan et al. 2003), in the optical domain. On the other hand, the XNOR gate is widely involved in various signal processing tasks in the binary world. These include data encoding (Wang et al. 2007), single (Wang et al. 2007) and multi-bit comparison (Scaffardi et al. 2008), binary pattern recognition (Webb et al. 2009) and matching (Ahn et al. 1999), basic Boolean arithmetic operations (Scaffardi et al. 2008) and optical code division multiple access (Ghaffari and Salehi 2009).

5 Conclusion

In this study, the performance of all-optical NOR and XNOR operations with the nonlinear effect of two-photon absorption (TPA) in quantum-dot semiconductor optical amplifiers (QDSOAs)-based Mach–Zehnder interferometers was numerically studied at

2 Tb/s. The results show that a higher quality factor is obtained when including the TPA effect, which contributes to the ultrafast QD carrier dynamics.

Acknowledgements This work was funded by the Chinese Academy of Sciences President's International Fellowship Initiative (PIFI) (Grant No. 2019FYT0002) and Talented Young Scientist Program (TYSP) supported by the China Science and Technology Exchange Center of Ministry of Science and Technology of China.

References

Ahn, K.H., Lou, J.W., Liang, Y., Boyraz, O., Xia, T.J., Kao, Y.H., Islam, M.N.: System performance measurements for an all-optical header processor using 100-Gb/s packets. IEEE Photon. Technol. Lett. **11**, 140–142 (1999)

Akiyama, T., Ekawa, M., Sugawara, M., Kawaguchi, K., Sudo, H., Kuramata, A., Ebe, H., Arakawa, Y.: An ultrawide-band semiconductor optical amplifier having an extremely high penalty-free output power of 23 dBm achieved with quantum dots. IEEE Photon. Technol. Lett. **17**, 1614–1616 (2005)

Berg, T.W., Bischoff, S., Magnusdottir, I., Mørk, J.: Ultrafast gain recovery and modulation limitations in self-assembled quantum-dot devices. IEEE Photon. Technol. Lett. **13**, 541–543 (2011)

Bilenca, A., Eisenstein, G.: On the noise properties of linear and nonlinear quantum-dot semiconductor optical amplifiers: the impact of inhomogeneously broadened gain and fast carrier dynamics. IEEE J. Quantum Electron. **40**, 690–702 (2004)

Breuer, D., Petermann, K.: Comparison of NRZ- and RZ-modulation format for 40-Gb/s TDM standard-fiber systems. IEEE Photon. Technol. Lett. **9**, 398–400 (1997)

Byun, Y.T., Kim, J.H., Jhon, Y.M., Lee, S., Woo, D.H., Kim, S.H.: High-speed all-optical NOR gate using semiconductor optical amplifier. In: Conference on Lasers and Electro-Optics Europe (2003)

Chan, L.Y., Qureshi, K.K., Wai, P.K.A., Moses, B., Lui, L.F.K., Tam, H.Y., Demokan, M.S.: All-optical bit-error monitoring system using cascaded inverted wavelength converter and optical NOR gate. IEEE Photon. Technol. Lett. **15**, 593–595 (2003)

Chen, X., Huo, L., Zhao, Z., Zhuang, L., Lou, C.: Study on 100-Gb/s reconfigurable all-optical logic gates using a single semiconductor optical amplifier. Opt. Express **24**, 30245–30253 (2016)

Dimitriadou, E., Zoiros, K.E.: On the design of reconfigurable ultrafast all-optical NOR and NAND gates using a single quantum-dot semiconductor optical amplifier-based Mach–Zehnder interferometer. J. Opt. **14**, 105401 (2012a)

Dimitriadou, E., Zoiros, K.E.: Proposal for all-optical NOR gate using single quantum-dot semiconductor optical amplifier-based Mach–Zehnder interferometer. Opt. Commun. **285**, 1710–1716 (2012b)

Dimitriadou, E., Zoiros, K.E.: Proposal for ultrafast all-optical XNOR gate using single quantum-dot semiconductor optical amplifier-based Mach–Zehnder interferometer. Opt. Laser Technol. **45**, 79–88 (2013)

Dong, J., Zhang, X., Xu, J., Huang, D.: 40 Gb/s all-optical logic NOR and OR gates using a semiconductor optical amplifier: experimental demonstration and theoretical analysis. Opt. Commun. **281**, 1710–1715 (2008)

Dorren, H.J.S., Khoe, G.D., Lenstra, D.: All-optical switching of an ultrashort pulse using a semiconductor optical amplifier in a Sagnac-interferometric arrangement. Opt. Commun. **205**, 247–252 (2002)

Dorren, H.J.S., Yang, X., Lenstra, D., deWaardt, H., Khoe, G.D., Simoyama, T., Ishikawa, H., Kawashima, H., Hasama, T.: Ultrafast refractive-index dynamics in a multi-quantum-well semiconductor optical amplifier. IEEE Photon. Technol. Lett. **15**, 792–794 (2003)

Dorren, H.J.S., Yang, X., Mishra, A.K., Li, Z., Ju, H., deWaardt, H., Khoe, G.D., Simoyama, T., Ishikawa, H., Kawashima, H., Hasama, T.: All-optical logic based on ultrafast gain and index dynamics in a semiconductor optical amplifier. IEEE J. Sel. Top. Quantum Electron. **10**, 1079–1092 (2004)

Durhuus, T., Mikkelsen, B., Joergensen, C., Danielsen, S.L., Stubkjaer, K.E.: All-optical wavelength conversion by semiconductor optical amplifiers. J. Lightwave Technol. **14**, 942–954 (1996)

Dutta, N.K., Wang, Q.: Semiconductor Optical Amplifiers, 2nd edn. World Scientific Publishing Company, Singapore (2013)

Folliot, H., Lynch, M., Bradley, A.L., Krug, T., Dunbar, L.A., Hegarty, J., Donegan, J.F.: Two-photon-induced photoconductivity enhancement in semiconductor microcavities: a theoretical investigation. J. Opt. Soc. Am. B **19**, 2396–2402 (2002)

Ghaffari, B.M., Salehi, J.A.: Multiclass, multistage, and multilevel fiber-optic CDMA signaling techniques based on advanced binary optical logic gate elements. IEEE Trans. Commun. **57**, 1424–1432 (2009)
Grillot, F., Veselinov, K., Gioannini, M., Montrosset, I., Even, J., Piron, R., Homeyer, E., Loualiche, S.: Spectral analysis of 1.55 μm InAs-InP(113)B quantum-dot lasers based on a multipopulation rate equations model. IEEE J. Quantum Electron. **45**, 872–878 (2009)
Han, B., Liu, Y.: All-optical reconfigurable non-inverted logic gates with a single semiconductor optical amplifier. AIP Adv. **9**, 015007 (2019)
Hong, M.Y., Chang, Y.H., Dienes, A., Heritage, J.P., Delfyett, P.J., Dijaili, S., Patterson, F.G.: Femtosecond self- and cross-phase modulation in semiconductor laser amplifiers. IEEE J. Sel. Top. Quantum Electron. **2**, 523–539 (1996)
Hu, H., Zhang, X., Zhao, S.: High-speed all-optical logic gate using QD-SOA and its application. Cogent Phys. **4**(1388156), 1–21 (2017)
Ju, H., Uskov, A.V., Notzel, R., Li, Z., Vazquez, J.M., Lenstra, D., Khoe, G.D., Dorren, H.J.S.: Effects of two-photon absorption on carrier dynamics in quantum-dot optical amplifiers. Appl. Phys. B **82**, 615–620 (2006)
Jung, Y.J., Son, C.W., Jhon, Y.M., Lee, S., Park, N.: One-level simplification method for all-optical combinational logic circuits. IEEE Photon. Technol. Lett. **20**, 800–802 (2008)
Kang, I., Rasras, M., Buhl, L., Dinu, M., Cabot, S., Cappuzzo, M., Gomez, L.T., Chen, Y.F., Patel, S.S., Dutta, N., Piccirilli, A., Jaques, J., Giles, C.R.: All-optical XOR and XNOR operations at 86.4 Gb/s using a pair of semiconductor optical amplifier Mach-Zehnder interferometers. Opt. Express **17**, 19062–19065 (2009)
Kim, J.H., Kim, Y.I., Byun, Y.T., Jhon, Y.M., Lee, S., Kim, S.H., Woo, D.H.: All-optical logic gates using semiconductor optical-amplifier-based devices and their applications. J. Korean Phys. Soc. **45**, 1158–1161 (2004)
Kim, J.Y., Kang, J.M., Kim, T.Y., Han, S.K.: All-optical multiple logic gates with XOR, NOR, OR and NAND function using parallel SOA-MZI structures: theory and experiment. J. Lightwave Technol. **24**, 3392–3399 (2006a)
Kim, J.Y., Kang, J.M., Kim, T.Y., Han, S.K.: 10 Gbits all-optical composite logic gates with XOR, NOR, OR and NAND functions using SOA-MZI structures. Electron. Lett. **42**, 303–307 (2006b)
Kim, J., Laemmlin, M., Meuer, M., Bimberg, D., Eisenstein, G.: Theoretical and experimental study of high-speed small-signal cross-gain modulation of quantum-dot semiconductor optical amplifiers. IEEE J. Quantum Electron. **45**, 240–248 (2009)
Kotb, A.: All-Optical Logic Gates Using Semiconductor Optical Amplifier. Lambert Academic Publishing, Saarbrucken (2012)
Kotb, A.: 1 Tb/s high-quality factor NOR gate based on quantum-dot semiconductor optical amplifier. Opt. Quantum Electron. **45**, 1258–1268 (2013)
Kotb, A.: Performance of all-optical XNOR gate based on two-photon absorption in semiconductor optical amplifiers. Adv. Opt. Technol. **2014**, 754713 (2014)
Kotb, A.: Simulation of all-optical logic NOR gate based on two-photon absorption with semiconductor optical amplifier-assisted Mach–Zehnder interferometer with the effect of amplified spontaneous emission. J. Korean Phys. Soc. **66**, 1593–1598 (2015a)
Kotb, A.: Modeling of high-quality-factor XNOR gate using quantum-dot semiconductor optical amplifiers at 1 Tb/s. Braz. J. Phys. **45**, 288–295 (2015b)
Kotb, A.: Theoretical analysis of soliton NOR gate with semiconductor optical amplifier-assisted Mach–Zehnder interferometer. Opt. Quantum Electron. **49**, 1–12 (2017a)
Kotb, A.: Computational analysis of soliton all-optical logic NAND and XNOR gates using semiconductor optical amplifiers. Opt. Quantum Electron. **49**, 1–17 (2017b)
Kotb, A., Guo, C.: Two-photon absorption in quantum dot semiconductor optical amplifiers-based all-optical XOR gate at 2 Tb/s. Opt. Quantum Electron. **51**, 1–12 (2019)
Kotb, A., Zoiros, K.E.: Simulation of all-optical logic XNOR gate based on quantum-dot semiconductor optical amplifiers with amplified spontaneous emission. Opt. Quantum Electron. **45**, 1213–1222 (2013)
Kotb, A., Zoiros, K.E., Guo, C.: All-optical XOR, NOR, and NAND logic functions with parallel semiconductor optical amplifier-based Mach–Zehnder interferometer modules. Opt. Laser Technol. **108**, 426–433 (2018)
Kotb, A., Zoiros, K.E., Guo, C.: 2 Tb/s all-optical gates based on two-photon absorption in quantum dot semiconductor optical amplifiers. Opt. Laser Technol. **112**, 442–451 (2019)
Lee, S., Park, J., Lee, K., Eom, D., Lee, S., Kim, J.H.: All-optical exclusive NOR logic gate using Mach–Zehnder interferometer. Jpn. J. Appl. Phys. **41**, 1155–1157 (2002)

Li, W., Ma, S., Hu, H., Dutta, N.K.: All-optical latches based on two-photon absorption in semiconductor optical amplifiers. J. Opt. Soc. Am. B **29**, 2603–2609 (2012)

Li, W., Hu, H., Zhang, X., Dutta, N.K.: High speed all optical logic gates using binary phase shift keyed signal based on QD-SOA. Int. J. High Speed Electron. Syst. **24**(1550005), 1–25 (2015)

Ma, S., Sun, H., Chen, Z., Dutta, N.K.: High-speed all-optical PRBS generation based on quantum-dot semiconductor optical amplifiers. Opt. Express **17**, 18469–18477 (2009)

Meuer, C., Schmeckebier, H., Fiol, G., Arsenijevic, D., Kim, J., Eisenstein, G., Bimberg, D.: Cross-gain modulation and four-wave mixing for wavelength conversion in undoped and p-doped 1.3 μm quantum dot semiconductor optical amplifiers. IEEE J. Photon. **2**, 141–151 (2010)

Pereira, A., Ostermann, F., Cavalcanti, C.: On the use of a virtual Mach-Zehnder interferometer in the teaching of quantum mechanics. Phys. Educ. **44**, 281–291 (2009)

Qasaimeh, O.: Optical gain and saturation characteristics of quantum dot semiconductor optical amplifiers. IEEE J. Quantum Electron. **39**, 793–798 (2003)

Scaffardi, M., Andriolli, N., Meloni, G., Berrettini, G., Fresi, F., Castoldi, P., Potì, L., Bogoni, A.: Photonic combinatorial network for contention management in 160 Gb/s-interconnection networks based on all-optical 2×2 switching elements. IEEE J. Sel. Top. Quantum Electron. **13**, 1531–1539 (2007)

Scaffardi, M., Ghelfi, P., Lazzeri, E., Potı, L., Bogoni, A.: Photonic processing for digital comparison and full addition based on semiconductor optical amplifiers. IEEE J. Sel. Top. Quantum Electron. **14**, 826–833 (2008)

Sharaiha, A., Topomondzo, J., Morel, P.: All-optical logic AND–NOR gates with three inputs based on cross-gain modulation in a semiconductor optical amplifier. Opt. Commun. **265**, 322–325 (2006)

Singh, S., Lovkesh, : Ultrahigh-speed optical signal processing logic based on an SOA-MZI. IEEE J. Sel. Top. Quantum Electron. **18**, 970–975 (2012)

Sugawara, M., Hatori, N., Ishida, M., Ebe, H., Arakawa, Y., Akiyama, T., Otsubo, K., Yamamoto, T., Nakata, Y.: Recent progress in self-assembled quantum-dot optical devices for optical telecommunication: temperature-insensitive 10 Gb/s directly modulated lasers and 40 Gb/s signal-regenerative amplifiers. J. Phys. D **38**, 2126–2134 (2005)

Sun, H., Wang, Q., Dong, H., Dutta, N.K.: XOR performance of a quantum dot semiconductor optical amplifier based Mach–Zehnder interferometer. Opt. Express **13**, 1892–1899 (2005)

Sun, H., Chen, Z., Ma, S., Dutta, N.K.: All-optical logic NOR gate at 40 Gb/s using SOA-based Mach-Zehnder interferometer. Proc. SPIE 6775, 67750F (2007)

Thapa, S., Zhang, X., Dutta, N.K.: Effects of two-photon absorption on pseudo-random bit sequence operating at high speed. J. Mod. Opt. **66**, 100–108 (2019)

van der Poel, M., Gehrig, E., Hess, O., Birkedal, D., Hvam, J.M.: Ultrafast gain dynamics in quantum-dot amplifiers: theoretical analysis and experimental investigations. IEEE J. Quantum Electron. **41**, 1115–1123 (2005)

Wang, Q., Zhu, G., Chen, H., Jaques, J., Leuthold, J., Piccirilli, A.B., Dutta, N.K.: Study of all-optical XOR using Mach–Zehnder interferometer and differential scheme. IEEE J. Quantum Electron. **40**, 703–710 (2004)

Wang, Y., Zhang, X., Dong, J., Huang, D.: Simultaneous demonstration on all optical digital encoder and comparator at 40 Gb/s with semiconductor optical amplifiers. Opt. Express **15**, 15080–15085 (2007)

Webb, R.P., Yang, X., Manning, R.J., Maxwell, G.D., Poustie, A.J., Lardenois, S., Cotter, D.: All optical binary pattern recognition at 42 Gb/s. J. Lightwave Technol. **27**, 2240–2245 (2009)

Xiao, J.L., Huang, Y.Z.: Numerical analysis of gain saturation, noise figure, and carrier distribution for quantum-dot semiconductor-optical amplifiers. IEEE J. Quantum Electron. **44**, 445–448 (2008)

Xu, J., Zhang, X., Liu, D., Huang, D.: Ultrafast all-optical NOR gate based on semiconductor optical amplifier and fiber delay interferometer. Opt. Express **14**, 10708–10714 (2006)

Xu, J., Zhang, X., Dong, J., Liu, D., Huang, D.: Simultaneous all-optical AND and NOR gates for NRZ differential phase-shift-keying signals. IEEE Photon. Technol. Lett. **20**, 596–598 (2008)

Zhang, X., Dutta, N.K.: Effects of two-photon absorption on all-optical logic operation based on quantum-dot semiconductor optical amplifiers. J. Mod. Opt. **65**, 166–173 (2018)

Zhang, X., Li, W., Hu, H., Dutta, N.K.: High-speed all-optical encryption and decryption based on two-photon absorption in semiconductor optical amplifiers. J. Opt. Commun. Netw. **7**, 276–285 (2015)

Zhang, X., Thapa, S., Dutta, N.K.: All-optical XOR gates based on dual semiconductor optical amplifiers. Cogent Phys. **6**(1660495), 1–14 (2019)

Zilkie, A.J., Meier, J., Mojahedi, M., Poole, P.J., Barrios, P., Poitras, D., Rotter, T.J., Yang, C., Stintz, A., Malloy, K.J., Smith, P.W.E., Aitchison, J.S.: Carrier dynamics of quantum-dot, quantum-dash and quantum-well semiconductor optical amplifiers operating at 1.55 μm. IEEE J. Quantum Electron. **43**, 982–991 (2007)